



HAL
open science

Comparative Secretome Analysis of *Ralstonia solanacearum* Type 3 Secretion-Associated Mutants Reveals a Fine Control of Effector Delivery, Essential for Bacterial Pathogenicity

Fabien Lonjon, Marie Turner, Celine C. Henry, David Rengel, David Lohou, Quitterie van de Kerkhove, Anne-Claire Cazalé, Nemo Peeters, Stéphane Genin, Fabienne Vailleau

► To cite this version:

Fabien Lonjon, Marie Turner, Celine C. Henry, David Rengel, David Lohou, et al.. Comparative Secretome Analysis of *Ralstonia solanacearum* Type 3 Secretion-Associated Mutants Reveals a Fine Control of Effector Delivery, Essential for Bacterial Pathogenicity. *Molecular and Cellular Proteomics*, 2016, 15, pp.598-616. hal-02634767

HAL Id: hal-02634767

<https://hal.inrae.fr/hal-02634767>

Submitted on 27 May 2020

HAL is a multi-disciplinary open access archive for the deposit and dissemination of scientific research documents, whether they are published or not. The documents may come from teaching and research institutions in France or abroad, or from public or private research centers.

L'archive ouverte pluridisciplinaire **HAL**, est destinée au dépôt et à la diffusion de documents scientifiques de niveau recherche, publiés ou non, émanant des établissements d'enseignement et de recherche français ou étrangers, des laboratoires publics ou privés.

Comparative Secretome Analysis of *Ralstonia solanacearum* Type 3 Secretion-Associated Mutants Reveals a Fine Control of Effector Delivery, Essential for Bacterial Pathogenicity*

Fabien Lonjon‡§, Marie Turner‡§, Céline Henry¶, David Rengel‡§, David Lohou‡§, Quitterie van de Kerkhove‡§, Anne-Claire Cazalé‡§, Nemo Peeters‡§, Stéphane Genin‡§, and Fabienne Vaillau‡§**

Ralstonia solanacearum, the causal agent of bacterial wilt, exerts its pathogenicity through more than a hundred secreted proteins, many of them depending directly on the functionality of a type 3 secretion system. To date, only few type 3 effectors have been identified as required for bacterial pathogenicity, notably because of redundancy among the large *R. solanacearum* effector repertoire. In order to identify groups of effectors collectively promoting disease on susceptible hosts, we investigated the role of putative post-translational regulators in the control of type 3 secretion. A shotgun secretome analysis with label-free quantification using tandem mass spectrometry was performed on the *R. solanacearum* GMI1000 strain. There were 228 proteins identified, among which a large proportion of type 3 effectors, called Rip (Ralstonia injected proteins). Thanks to this proteomic approach, RipBJ was identified as a new effector specifically secreted through type 3 secretion system and translocated into plant cells. A focused Rip secretome analysis using *hpa* (hypersensitive response and pathogenicity associated) mutants revealed a fine secretion regulation and specific subsets of Rips with different secretion patterns. We showed that a set of Rips (RipF1, RipW, RipX, RipAB, and RipAM) are secreted in an Hpa-independent manner. We hypothesize that these Rips could be preferentially involved in the first stages of type 3 secretion. In addition, the secretion of about thirty other Rips is controlled by HpaB and HpaG. HpaB, a candidate chaperone was shown to positively control secretion of numerous

Rips, whereas HpaG was shown to act as a negative regulator of secretion. To evaluate the impact of altered type 3 effectors secretion on plant pathogenesis, the *hpa* mutants were assayed on several host plants. HpaB was required for bacterial pathogenicity on multiple hosts whereas HpaG was found to be specifically required for full *R. solanacearum* pathogenicity on the legume plant *Medicago truncatula*. *Molecular & Cellular Proteomics* 15: 10.1074/mcp.M115.051078, 598–613, 2016.

The soil-borne vascular bacterium *R. solanacearum* is described as one of the most destructive plant pathogenic bacterium worldwide (1), mainly because of its broad host range and wide geographic distribution. Indeed, *R. solanacearum* attacks more than 250 plant species, distributed in more than 50 botanical families (2). *R. solanacearum* causes dramatic crop losses, more specifically in the tropics, notably affecting emerging countries. Durable protection strategies against this bacterium are lacking. *R. solanacearum* penetrates into the plant *via* the roots, and then colonizes the xylem vessels. The bacterium reaches the aerial parts of the plant, causes wilting symptoms leading to the death of the plant, and will eventually return to the soil, completing the cycle (3). To achieve these first colonization steps, the bacterium uses a molecular syringe called the type 3 secretion system (T3SS),¹ which de-

From the ‡INRA, Laboratoire des Interactions Plantes-Microorganismes (LIPM), UMR441, Castanet-Tolosan, F-31326, France; §CNRS, Laboratoire des Interactions Plantes-Microorganismes (LIPM), UMR2594, Castanet-Tolosan, F-31326, France; ¶PAPPSO, Micalis Institute, INRA, AgroParisTech, Université Paris-Saclay, 78350 Jouy-en-Josas, France; ||Université de Toulouse; INP; ENSAT; 18 chemin de Borde Rouge, Castanet Tolosan, 31326, France

Received May 7, 2015, and in revised form, September 17, 2015
 Published, MCP Papers in Press, December 3, 2015, DOI 10.1074/mcp.M115.051078

Author contributions: F.L., M.T., C.H. and F.V. Designed Research; F.L., M.T., C.H., D.L., Q.K. and F.V. Performed Research; F.L., M.T., C.H., D.R., A.C.C., N.P., S.G. and F.V. Contributed new reagents or analytic tools; F.L., C.H., D.R. and F.V. Analyzed data; F.L., C.H., D.R., N.P., S.G. and F.V. Wrote or contributed to the writing of the paper.

¹ The abbreviations used are: T3SS, Type 3 secretion system; cAMP, cyclic adenosine monophosphate; glht, general linear hypothesis test; hrc, hypersensitive response and pathogenicity conserved; hrp, hypersensitive response and pathogenicity; hpa, hypersensitive response and pathogenicity associated; HA, human influenza hemagglutinin; kDa, kilo dalton; LC-MS/MS, liquid chromatography–tandem mass spectrometry; m/z, mass-to-charge ratio; MS, mass spectra from precursor ion; MS2, fragmentation mass spectra; MW, molecular weight; OD, optical density; PAI, protein abundance index; PCA, principal component analysis; ppm, part per million; Rip, Ralstonia injected protein; rpkm, reads per kilobase per million mapped reads; rpm, rotation per minute; SC, spectral counting; T3, type 3; T3C, type 3 chaperone; T3E, type 3 effector; T3S, type 3 secretion; T3S4, type 3 secretion substrate switch specificity; TCA, trichloroacetic acid; Th, thomson unit; v/v, volume to volume ratio.

livers virulence factors, the type 3 effectors (T3Es) into the host cells. Collectively, these effectors constitute one of the main weapons of the pathogenicity arsenal of *R. solanacearum*, as it is the case for many other Gram-negative phytopathogenic bacteria (i.e. *Pseudomonas* spp., *Xanthomonas* spp., and *Erwinia* spp.) (4). Many early substrates of the secretion apparatus are highly conserved among these bacteria, including the cytoplasmic, inner and outer membrane ring components, and the needle. The translocators (intermediate substrates) and the translocated effectors (late substrates) show more diversity, which may contribute to the host specificities of each pathogenic bacterium (4–6). The core component proteins are encoded by the *hrp* (hypersensitive response and pathogenicity) and *hrc* (*hrp*-conserved) genes, located on the *hrp* gene cluster, whereas the T3Es are distributed throughout the genomes of these bacteria (7–10).

R. solanacearum strains possess large T3E repertoires, with 72 Rips (Ralstonia injected proteins) identified in the model strain GMI1000 (11). Rip delivery through the T3SS is under a fine transcriptional control, orchestrated by the regulatory protein HrpB. This transcription factor activates both the expression of the T3SS encoding genes and of the T3E genes (12). The *R. solanacearum* T3SS transcriptional regulatory system is well described (13), whereas little is known about the post-translational control of Rip delivery. There were 94 Rip genes identified among strains of the *R. solanacearum* species complex sequenced to date (11). This large repertoire of virulence factors may explain the wide host range of this bacterium. However, because of Rip redundancy (14–16), single Rip are often dispensable for bacterial pathogenicity on a given host, except for RipG7 (formerly named GALA7) on the legume plant *Medicago truncatula* (17). To date, many questions remain, we still do not know whether there could be a specific regulation of Rip delivery, depending on the host plant, the host tissues, or on the stage of bacterial colonization. Are all Rips delivered into the host at the same time, in equal quantities, or is there a hierarchical and quantitative control?

To better understand this complex mechanism, we studied the delivery of Rips via the T3SS through *in vitro* Rip secretion. We used optimized secretion conditions (18) in which the bacterium is in an HrpB-inducing environment, mimicking the *in planta* conditions and leading to Rip secretion. With this standardized and controlled system, we aimed at identifying sets of Rips with conserved and typical secretion patterns. Like it has been shown for other pathogenic bacteria (19, 20), we can hypothesize that Rip delivery is post-translationally controlled by helper proteins. These helper proteins are described in both plant and animal pathogenic bacteria, but are not orthologs. They are known to regulate T3E transit through the T3SS at post-transcriptional and post-translational levels, stabilizing T3Es, preventing their degradation or ordering and mediating their recognition by the T3SS (19, 21, 22). Some secretion helper proteins have been well described, like the T3Cs (type 3 chaperones), or the T3S4 (type 3 secretion

substrate specificity switch) proteins (6, 22). Our previous work on *R. solanacearum* HpaP, a putative T3S4 protein, revealed that this regulatory protein could act as a modulator of the secretion level, targeting some T3Es, notably via direct protein interactions (23).

To advance our knowledge on the *R. solanacearum* T3S and on its post-translational control, we explored the complete secretome of *R. solanacearum*, taking advantage of the most recent tandem MS approach. In this work, we describe the most complete secretome (228 proteins including Rips) of a plant pathogenic bacterium using a MS-based shotgun approach with a label-free quantification (24). This allowed us to compare secretomes between *hpa* (*hrp*-associated) mutants and evaluate their respective involvement in T3S. In parallel, the phenotypic analysis of these *hpa* mutants on different host plants was carried out. This first in-depth proteomic approach on *R. solanacearum* enhances our knowledge on the T3S regulation and is a new mean to identify sets of Rips potentially coregulated, likely to be relevant for host specificity.

EXPERIMENTAL PROCEDURES

Bacterial Strains, Plasmids, and Growth Conditions—The bacterial strains used in this work are listed in Table I. *Escherichia coli* strains were grown at 37 °C in Luria-Bertani medium. *Ralstonia solanacearum* strains were grown in complete B medium or minimal medium, as previously described (25). When needed, antibiotics were added at the following final concentrations (mg/L): kanamycin (50), spectinomycin (40), gentamycin (10), tetracycline (10) for *R. solanacearum* and kanamycin (25), spectinomycin (40), gentamycin (10), tetracycline (10), ampicillin (50), chloramphenicol (25) for *E. coli*. The plasmids used in this study, listed in Table I, were constructed by Gateway technology (Life Technologies, Carlsbad, CA) following the instructions of the manufacturer. Genes cloned in the pDONR207 plasmid were amplified in two steps. The first PCR was performed using the specific primers indicated in Supplemental Experimental Procedures. The second PCR was performed using 1 μl of the first PCR as matrix and attB universal primers (oNP291 5'-GGGGACA-AGTTTGTACAAAAAAGCAGGCTTCGAAGGAGATAGAACCATG-3' and oNP292 5'-GGGGACCACTTTGTACAAGAAAGCTGGGTC-3').

Generation of *R. solanacearum* Mutants—*R. solanacearum* mutants are listed in Table I. *hrcV*, *hpaG*, and *hpaD* mutants were previously generated (12). In this study we constructed *hpaB* and *ripBJ* (*RSp0213*) mutants. To generate *hpaB* mutation in the GMI1000 wild-type strain, a 1.6 kb DNA fragment encompassing *hpaB* was PCR-amplified using the following primers G-UPLNG 5'-AAGCTTC-CCGGACGGCTCAACGC-3' and HPAB-rev 5'-AAGCTTGTAGATGT-GCTGCTCGA-3' and then cloned into the pUC18 vector. The Ω-spectinomycin interposon (26) was cloned into the unique NotI restriction site within the *hpaB* open reading frame to generate plasmid pSG424. pSG424 was linearized by XbaI and used to transform *R. solanacearum* as previously described (27). Strain GRS474 was obtained by selecting a double recombination event using spectinomycin resistance and *hpaB* gene disruption was then checked by PCR. The same strategy was used to generate the strain GRS503 (*RSp0213* mutant). p213fw 5'-TCTAGATCCAGGTGGCGCTGCAG-3' and p213rev 5'-GTTTCGACGTGGATGCGGGC-3' primers were used to amplify and clone a 1.6 kb fragment containing *RSp0213* into the pUC vector. The Ω-spectinomycin interposon (26) was cloned into the SmaI restriction site of *RSp0213* (pSG493). Transformation into *R.*

TABLE I

Strains and plasmids used in this study. **Cm^r*, *Gm^r*, *Km^r*, *Tc^r* and *Sp^r*, resistances to chloramphenicol, gentamycin, kanamycin, tetracycline and spectinomycin, respectively

	Characteristics	Source
<i>R. solanacearum</i> strains		
GMI1000	Wild-type strain	(8)
GMI1694	GMI1000 <i>hrcV</i> :: Ω mutant, <i>Sp^r</i>	(37)
GRS230	GMI1000 Δ <i>hpaG</i> mutant, <i>Gm^r</i>	(37)
GRS266	GMI1000 <i>hpaD</i> :: Ω mutant, <i>Sp^r</i>	(37)
GRS474	GMI1000 <i>hpaB</i> :: Ω mutant, <i>Sp^r</i>	This study
GRS503	GMI1000 <i>Rsp0213</i> :: Ω mutant, <i>Sp^r</i>	This study
Plasmids used for cloning		
pENTR/D-TOPO	Gateway™ entry vector, <i>Km^r</i>	Life Technologies
pENTR/SD/D-TOPO	Gateway™ entry vector, Shine–Dalgarno sequence, <i>Km^r</i>	Life Technologies
pDONR207	Gateway™ entry vector, <i>Gm^r</i> <i>Cm^r</i>	Life Technologies
pAA3	pENTR/D-TOPO derivating carrying <i>ripD</i> , <i>Km^r</i>	This study
pACC109	pDONR207 derivating carrying <i>ripH2</i> , <i>Gm^r</i>	This study
pACC220	pDONR207 derivating carrying <i>ripAN</i> , <i>Gm^r</i>	This study
pACC351	pDONR207 derivating carrying <i>ripH3</i> , <i>Gm^r</i>	This study
pACC387	pDONR207 derivating carrying <i>ripH1</i> , <i>Gm^r</i>	This study
pACC478	pDONR207 derivative carrying <i>ripW</i> , <i>Gm^r</i>	This study
pACC646	pENTR/SD/D-TOPO derivating <i>hpaG</i> , <i>Km^r</i>	This study
pACC702	pENTR/SD/D-TOPO derivating carrying <i>ripAB</i> , <i>Km^r</i>	This study
pACC750	pENTR/SD/D-TOPO derivating carrying <i>RSp0213</i> , <i>Km^r</i>	This study
pFL12	pMT1 derivatives carrying a <i>KpnI-HindIII</i> fragment of pNP224 containing the <i>ripG7</i> promoter <i>Km^r</i>	This study
pFL13	pLAFR6 carrying pFL12 <i>Tc^r</i> <i>Km^r</i>	This study
pLAFR6	pLAFR1 with <i>trp</i> terminators <i>Tc^r</i>	(25)
pLBy5	pDONR207 derivating carrying <i>hpaB</i> , <i>Gm^r</i>	This study
pLBy14	pDONR207 derivating carrying <i>ripAV</i> , <i>Gm^r</i>	This study
pMT1	pSC205 derivative carrying <i>CyaA4</i> –1197 N-terminal part, <i>Km^r</i>	(23)
pNP224	pSC205 derivative carrying <i>ripG7</i> promoter (from RSc1445146 to RSc1445497) upstream of the Gateway™ cassette <i>Km^r</i>	This study
pNP329	pRCG derivative (63) with the <i>RipG7</i> promoter followed by a Gateway™ destination cassette and a triple HA epitope tag, <i>Gm^r</i> <i>Km^r</i>	(23)
pSC205	pET26b(+) (Clontech) carrying a Gateway™ cassette <i>Km^r</i>	(23)
Plasmids for transformation in <i>R. solanacearum</i>		
pACC618	pNP329 derivative carrying <i>ripH2</i> , <i>Gm^r</i> <i>Km^r</i>	This study
pACC619	pNP329 derivative carrying <i>ripH3</i> , <i>Gm^r</i> <i>Km^r</i>	This study
pACC636	pNP329 derivative carrying <i>ripH1</i> , <i>Gm^r</i> <i>Km^r</i>	This study
pAM5	pLAFR3 carrying 2-kb fragment containing <i>hprB</i> , <i>Tc^r</i>	(18)
pEG3	pNP329 derivative carrying <i>ripAV</i> , <i>Gm^r</i> <i>Km^r</i>	This study
pEG4	pNP329 derivative carrying <i>ripW</i> , <i>Gm^r</i> <i>Km^r</i>	This study
pEG5	pNP329 derivative carrying <i>ripAN</i> , <i>Gm^r</i> <i>Km^r</i>	This study
pEG7	pNP329 derivative carrying <i>ripD</i> , <i>Gm^r</i> <i>Km^r</i>	This study
pEG8	pNP329 derivative carrying <i>hpaG</i> , <i>Gm^r</i> <i>Km^r</i>	This study
pEG10	pNP329 derivative carrying <i>ripAB</i> , <i>Gm^r</i> <i>Km^r</i>	This study
pEG11	pNP329 derivative carrying <i>hpaB</i> , <i>Gm^r</i> <i>Km^r</i>	This study
pFL11	pNP329 derivative carrying <i>RSp0213</i> , <i>Gm^r</i> <i>Km^r</i>	This study
pFL14	pFL13 derivative carrying <i>RSp0213</i> , <i>Tc^r</i> <i>Km^r</i>	This study

solanacearum was performed and checked as previously described for generation of GRS474 strain.

Construction of Strains with Effector-HA Tag and Complementation—Effector-3HA fusions were done using pNP329 (23) with the Gateway technology (Life Technologies) to allow stable chromosomal insertion. pNP329 derivatives carrying *ripD*, *ripH1*, *ripH2*, *ripH3*, *ripW*, *ripAB*, *ripAN*, and *ripAV*-3HA tags were linearized using *ScaI* enzyme, and then introduced into five strains, *i.e.* the wild-type (GMI1000) (8), and the *hrcV*, *hpaB*, *hpaD*, and *hpaG* mutants (GMI1694, GRS474, GRS266, and GRS230) by natural transformation as previously described (27). Stable chromosomal insertions in the defined bacterial chromosome site were checked by PCR using oNP611 5'-GAAAGCACGCTGTTCCGCTATTT-3', oNP612 5'-GCGTAGTGCG-CAAGACGAACAA-3' and oNP613 5'-GGCTCAAGGAGAAGAGC-

CTTCAGA-3' primers. The *hpaB* and *hpaG* mutants were complemented with their corresponding wild-type alleles, using pNP329 and the same procedure.

Secretome Sample Preparation—Five *R. solanacearum* strains were used for MS secretome analysis: GMI1000 wild-type strain, GMI1694 *hrcV* mutant, GRS474 *hpaB* mutant, GRS266 *hpaD* mutant and GRS230 *hpaG* mutant (Table I). These *R. solanacearum* strains carrying the pAM5 plasmid (18), that leads to a higher transcriptional activity of T3SS-regulated genes, were first cultivated in B medium overnight, pelleted for 5 min at 4000 rpm and then resuspended in 15 ml of minimal medium (supplemented with 0.1 g/L congo red and 10 mM glucose and 10 mM glutamate, with 10 μ g/ml tetracycline) at OD_{600 nm} = 0.2. Bacterial cultures were then harvested after 8 h of culture, set at the same concentration, according to the OD_{600 nm} and

pelleted for 10 min at 5000 rpm. One milliliter of supernatant was filter-sterilized (0.22 μm) and the proteins were precipitated using 1:1 (v/v) TCA 25%. The protein pellet was washed twice with acetone 90% and resuspended in 40 μl of Laemmli buffer with 0.2 M of Tris-HCl pH 7.4. Concentrated supernatants were then loaded onto a SDS-PAGE 10% bisacrylamid gel for a short migration. Portions of gels that contain the proteins (1 cm of sample migration) were cut for shotgun MS analysis.

Protein In-Gel Digestion—Each lane was cut and washed for 15 min with an acetonitrile/100 mM ammonium bicarbonate mixture (1:1). Digestion was performed in 50 mM ammonium bicarbonate pH 8.0 and the quantity of modified trypsin (Promega, sequencing grade, Madison, WI) was 0.1 μg per sample. Digestion was achieved for 6 h at 37 °C. The supernatant was conserved. Peptides were extracted by 5% formic acid in water/acetonitrile (v/v). Supernatant and extracted tryptic peptides were dried and resuspended in 50 μl of 0.1% (v/v) formic acid and 2% (v/v) acetonitrile.

Nano Liquid Chromatography Coupled to Mass Spectrometry in Tandem—A Q Exactive (Thermo Fisher Scientific) coupled to Eksigent 2Dnano LC (AB-Sciex, Framingham, MA) were used for the nano-LC-MS/MS analysis. Four microliters of sample were injected on the nanoLc-Ultra system (AB-Sciex) chain. Sample was loaded at 7.5 $\mu\text{l}/\text{min}$ on the precolumn cartridge (C18, 5 μm , 120 \AA , 20 mm Nanoseparations) and desalted with 0.1% formic acid. Then, peptides were separated with a gradient of acetonitrile on the reverse phase column C18 (stationary phase: C18 Biosphere, 3 μm ; column: 75 μm i.d., 150 mm; Nanoseparations). Buffers were 0.1% formic acid in water (A) and 0.1% formic acid in acetonitrile (B). The peptide separation was achieved with a linear gradient from 5 to 30% B for 40 min at 300 nL/min⁻¹. Eluted peptides were analyzed on-line with a Q Exactive mass spectrometer (Thermo Fisher Scientific, San Jose, CA) using a nanoelectrospray interface. Ionization (1.8 kV ionization potential) was performed with stainless steel emitters (30 μm i.d.; Thermo Fisher Scientific). Peptide ions were analyzed using Xcalibur 2.1 with the following data-dependent acquisition steps: (1) full MS scan (mass-to-charge ratio (m/z) 400 to 1400) and (2) MS/MS. Step two was repeated for the eight major ions detected in step one. Dynamic exclusion was set to 40 s. Lock mass option was chosen “best,” MS resolution 70,000 at m/z 400, auto gain control was 1e⁶, maximum injection time 250 ms. For MS2 the resolution was 17,500 at m/z 400, auto gain control was 2e⁵, maximum injection time 120 ms, isolation window m/z = 3, normalized collision energy: 30, underfill ratio 0.5%, intensity threshold 8.3e³. Charge state: 2, 3, 4; dynamic exclusion 40 s.

Data Processing and Bioinformatics Analysis—The *R. solanacearum* strain GMI1000 database was downloaded from Database site (<https://iant.toulouse.inra.fr/bacteria/annotation/cgi/ralso.cgi>, October 2012, 5122 protein entries). This database was merged and in conjunction with reverse and contaminant databases, were searched by X!Tandem (Sledge Hammer version 2013.09.01.1, <http://www.thegpm.org/tandem/>) using X!TandemPipeline (version 3.3.3) developed by PAPPISO platform (<http://pappiso.inra.fr/bioinfo/>). Enzymatic cleavage was declared as a trypsin digestion with one possible miss-cleavage. Cys carboxyamidomethylation and Met oxidation were set to static and possible modifications, respectively. Precursor mass was 10 ppm and fragment mass tolerance was 0.02 Th. A refinement search was added with similar parameters except for semitryptic peptides and possible N-ter proteins. For data of proteomic, only peptides with an E value smaller than 0.1 were reported. Identified proteins were filtered and grouped using X!TandemPipeline (<http://pappiso.inra.fr/bioinfo/xtandempipeline/>) according to: (1) a minimum of two different peptides was required with an E value smaller than 0.05, (2) a protein log (E value) (calculated as the product of unique peptide E values) smaller than 10⁻³. These criteria led to a

false discovery rate (FDR) of 0.08% for the wild-type strain and of 0.07% for the five strains (wild-type, *hrcV* and *hpa* mutants) for peptide and protein identification. To take redundancy into account, proteins with at least one peptide in common were grouped. This allowed to group proteins of similar function. Within each group, proteins with at least one specific peptide relatively to other members of the group were reported as subgroups. Only proteins detected on at least two samples on at least one strain were considered. Label-free quantification of proteins was achieved in two steps. The first one is the spectral counting (SC) (28–30), which is a strategy to determine a relative quantification of protein from their number of spectra obtained with tryptic peptides in MS. This quantification is based on the fact that the more of a particular protein is present in a sample, the more MS spectra are detected for peptides of that protein. The second step is performed using protein abundance index (PAI) for every protein and was obtained by dividing SC data of the observed protein by the number of theoretically observable tryptic peptides for that protein (31).

Experimental Design and Statistical Rationale—Concerning the secretome samples used for MS experiments, four independent biological replicates were generated for each of the five strains studied (wild-type strain, *hrcV*, *hpaB*, *hpaD*, and *hpaG* mutants). We found that four replicates were the best possible compromise in order to duly handle experimental variability and to do quantitative analysis. The *hrcV* mutant was used as a negative control of T3S, allowing discrimination of type 3 proteins. In order to be compared, samples were normalized dividing each PAI by the total sum of PAIs on the corresponding sample. Thus normalized PAI values were log-scaled to be able to adjust a linear model for every protein. With the aim of better handling multiple comparisons, general linear hypothesis tests (glht) (32) were subsequently run on the model to discriminate proteins differentially quantified between bacterial strains. All statistical procedures were carried out under [R] v3.1.1 environment (33) using base packages as well as “multcomp” (32), “limma” (34), and “venneuler” (35) packages. The R source code created for this study is available upon request.

Type 3 Secretion Assays and Immunoblot Analysis—The secretion pattern of thirteen T3Es was followed in five *R. solanacearum* backgrounds. First, the same five *R. solanacearum* strains as for MS experiments were used for secretion assays with available T3E specific antibodies. Second, for the other T3Es studied, T3E-HA fusions were generated (*ripD*, *ripH1*, *ripH2*, *ripH3*, *ripW*, *ripAB*, *ripAN*, and *ripAV*) and introduced into the five strains (see above). pAM5 (18) was added by electroporation into these 40 strains. Then, secretion assays were performed as previously described (23). Proteins from an equal amount of cultures (normalized by OD₆₀₀) were loaded in each lane. Total proteins were stained with Silver Stain Plus kit (Bio-Rad, Hercules, CA) (supplemental Fig. S1) or transferred to nitrocellulose membrane for Western blotting. Antibodies used were RipG7 (23), RipP1 (formerly PopP1) (36), RipP2 (formerly PopP2) (courtesy of L. Deslandes, INRA/CNRS, Castanet Tolosan, France), RipX (formerly PopA) (18), RipAA (formerly AvrA) (25), and an antihemagglutinin coupled with horseradish peroxidase (anti-HA) (Santa Cruz Biotechnology, Santa Cruz, CA). When needed, goat anti-rabbit antibody conjugated with horseradish peroxidase was used as secondary antibody (Santa Cruz Biotechnology, Santa Cruz, CA). Biologically independent experiments were performed twice.

Adenylate Cyclase (CyaA) Translocation Assays—A KpnI-HindIII fragment of pNP224 containing the *ripG7* promoter was cloned into pMT1 that carries *CyaA* 4–1197 N-terminal part (pFL12). Then pFL12 was cloned into the KpnI site of pLAFR6 to allow plasmid replication in *R. solanacearum* (pFL13). RSp0213 was then integrated into pFL13 by gateway cloning. RSp0213-CyaA¹ (pFL14) construct was transformed into GMI1000 (wild-type strain) and GMI1694 (*hrcV* mutant).

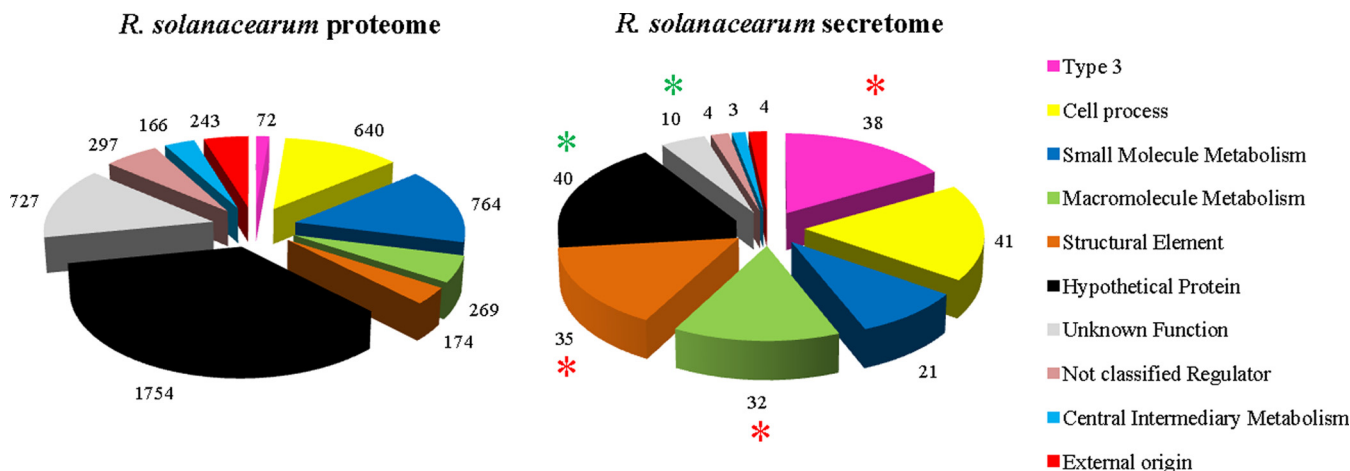


FIG. 1. *R. solanacearum* GMI1000 wild-type secretome shows enrichment in T3-proteins compared with the wild-type proteome. Distribution of total *R. solanacearum* proteins according to the predicted functions (<https://iant.toulouse.inra.fr/bacteria/annotation/cgi/ralso.cgi>) (left pie) compared with detected proteins by LC-MS/MS (right pie). Bonferroni-corrected hypergeometric tests (p values < 0.001) reveal three significantly enriched categories in the secretome (red asterisks), i.e. “Type 3” ($p = 5.72 \cdot 10^{-34}$), “Macromolecule Metabolism” ($p = 1.79 \cdot 10^{-6}$) and “Structural Element” ($p = 6.05 \cdot 10^{-13}$); as well as two significantly under-represented categories (green asterisks), i.e. “Hypothetical Protein” ($p = 1.06 \cdot 10^{-8}$) and “Unknown” ($p = 2.06 \cdot 10^{-5}$).

Translocation assays were performed as previously described on *Nicotiana tabacum* (37). The cAMP production was measured using the cAMP Biotrak enzyme immunoassay (EIA) System kit by GE Healthcare (Buckinghamshire, UK). Four independent biological replicates were performed.

Plant Assays and Statistical Analysis—For *Arabidopsis thaliana* assay, 16 Col-0 ecotype plants were inoculated as previously described (38) using 10^8 bacteria/ml, without cutting the roots. For *M. truncatula* (ecotype A17), two types of inoculation were performed. For soil inoculations, 16 *M. truncatula* plants with cut roots were soaked with 800 ml of a bacterial solution at 10^6 bacteria/ml. *In vitro* inoculations were done as previously described (39) with 10^7 bacteria/ml. Disease development was monitored every day, and plants with at least 50% of wilting were considered as dead for the statistical survival analysis. To compare the disease development of two given strains, we used the Kaplan-Meier survival analysis with the Gehan-Breslow-Wilcoxon test. A p value smaller than 0.05 was considered significant, indicating that the H_0 hypothesis of similarity of the survival experience of the tested strains can be rejected. Statistical analyses were done with Prism version 5.00 (GraphPad Software). Each experiment was repeated at least three times.

Internal Growth Curve—Internal Growth curve was determined mostly as previously described (39). Fourteen days post-inoculation, at least three pools of three plants were harvested, sterilized in 70% ethanol and rinsed three times in water. Plants were weighted, grinded and then resuspended in sterile water. Bacterial concentrations were determined by plating dilutions on B medium with antibiotic if necessary. Experiments were repeated three times.

RESULTS

Secretome of *R. solanacearum* GMI1000 Grown in Type 3 Secretion Inducing Conditions—Using LC-MS/MS, we analyzed the secretome of the *R. solanacearum* GMI1000 wild-type strain. Bacteria were grown in secretion inducing media, and four independent biological secretome samples were generated by a shotgun approach with label-free quantification. The experimental procedure scheme is shown in supplemental Fig. S2A. Identification of peptides was done using

X!TandemPipeline developed by PAPPISO platform (<http://pappiso.inra.fr/>). Protein identification was done using the *R. solanacearum* genome database (<https://iant.toulouse.inra.fr/bacteria/annotation/cgi/ralso.cgi>) and a contaminant database (trypsin, keratins, etc). A protein was considered as present in the supernatant when spectra were detected in at least two independent replicates. The number of spectra corresponding to each detected protein, the normalized protein abundance index (PAI), and all the peptide sequences are provided in supplemental Table S1. The analysis of strain GMI1000 secretome identified 228 proteins which were classified into functional groups according to the *R. solanacearum* proteome database (see supplemental Table S1; Fig. 1). A Bonferroni-corrected hypergeometric test (with a p value < 0.001) revealed a significant enrichment for three categories corresponding to macromolecule metabolism, structural elements, and type 3-associated proteins (Fig. 1). Among the 32 proteins belonging to the “macromolecule metabolism” class many previously characterized *R. solanacearum* secreted proteins were found, e.g. plant cell wall degrading enzymes (endo- and exoglucanases, polygalacturonases) (supplemental Table S1). The category of type 3-associated proteins showed the highest enrichment (p value = $5.72 \cdot 10^{-34}$). The 38 detected type 3-associated proteins included three structural elements of the syringe, the HrpY pilin (the major component of the Hrp pilus) and the two translocators RipF1_1 and RipF1_2 (formerly named PopF1 and PopF2), which are thought to form a pore in the plant cell (supplemental Fig. S2B). The 35 other type 3 proteins correspond to Rip protein effectors.

Type 3 Secretome of *R. solanacearum*—In order to define the set of T3-secreted proteins, we compared the GMI1000 wild-type secretome with the T3SS-defective *hrcV* mutant. There were 224 proteins detected in the *hrcV* mutant culture

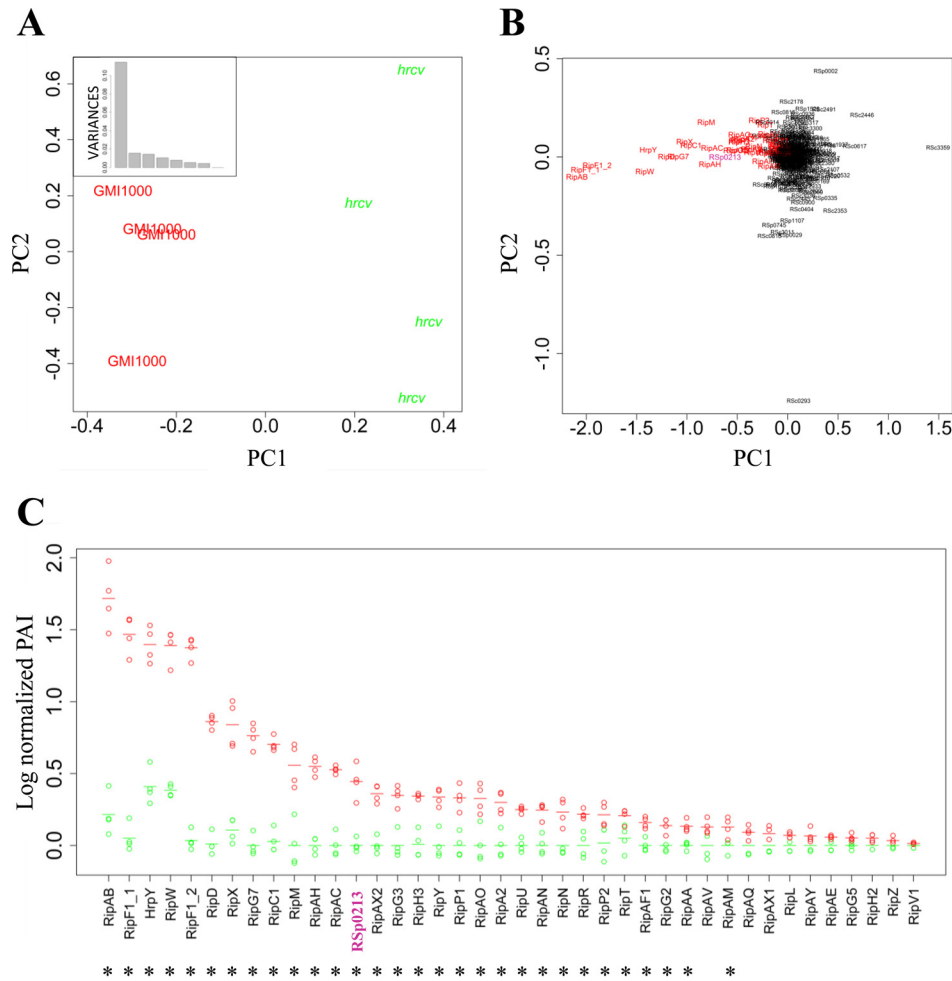


FIG. 2. *R. solanacearum* LC-MS/MS secretomes of GMI1000 wild-type strain and of *hrcV* mutant (a *hrp* defective mutant) bring specific and quantitative data on Rip secretion. A, PCA with the detected proteins in the wild-type strain and in the *hrcV* mutant highlights the strain effect on the first component, which presents a standard deviation of 0.34 and explains 66% of the total variance (box). B, protein distribution on the same PCA shows that the most discriminating proteins are T3-associated proteins (in red), and reveals a new Rip candidate: RSp0213 (in purple). C, log-normalized PAI values of T3-associated proteins detected in the wild-type (red) and in the *hrcV* mutant (green) secretomes. The proteins were classified according to their level of secretion in the wild-type strain (from the strongest to the lowest log-normalized PAI values). Four biological replicates were analyzed for each strain. Each dot represents a replicate; dashes represent the mean values of all four replicates. Asterisks highlight proteins presenting significantly different secretion levels between both strains (glht post-hoc test, p value < 0.05).

supernatant (supplemental Fig. S3). A principal component analysis (PCA) on log-normalized PAI data was carried out to identify and visualize the sources of variability between all eight analyzed samples (four for each bacterial strain). The PCA on Fig. 2A clearly shows that the “strain” effect defining the first principal component, explains 66% of the overall variation. The positioning of the individual proteins on the PCA highlights that variance on this first component is quasi-exclusively because of T3-associated proteins (Fig. 2B). A similar analysis conducted excluding the annotated T3-associated proteins, shows that the strain effect is still present (supplemental Fig. S4A), but in this case the first principal component only explains 30% of the overall variance (supplemental Fig. S4B), with very few discriminating proteins being responsible for this component (supplemental Fig.

S4C). A linear model was fitted and the subsequent glht post-hoc tests were performed to discriminate the proteins differentially secreted between GMI1000 and the *hrcV* mutant, revealing 63 proteins differentially secreted (p value < 0.05) (supplemental Table S2). Twenty-nine out of these 63 proteins were found to be T3-associated proteins (HrpY and 28 Rips). These 29 proteins are among the most significantly different between both strains with the lowest p values (supplemental Table S2). The secretion pattern of all the T3-proteins detected in both strains is shown in Fig. 2C. A noticeable point is that none or, at best, very few spectra were detected for any of the Rip T3Es (except RipW) in the *hrcV* mutant (supplemental Table S3, Fig. 2C). The barely detected T3S SC data on the *hrcV* replicates suggest a minimal bacterial lysis in our secretome samples. Overall, these first data can be considered as

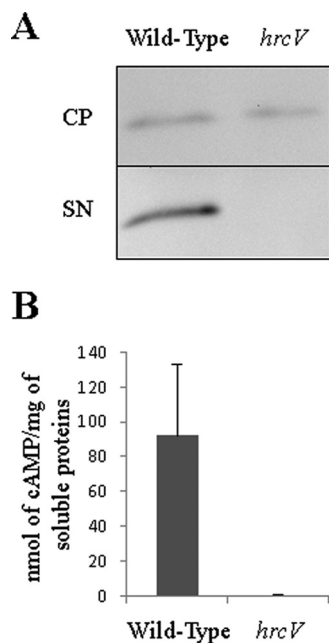


FIG. 3. RSp0213 is secreted and translocated through the T3SS.

A, the wild-type strain and the *hrcV* mutant were transformed to express RSp0213-HA fusion. Secretion assays were performed and total proteins from bacterial cell pellet (CP) and proteins in the supernatant (SN) were detected by Western-Blot. Detected signal size corresponds to the RSp0213-HA size (18 kDa). B, translocation assay of RSp0213 protein in *N. tabacum* leaves using RSp0213-CyaA' fusion protein. Cyclic adenosine monophosphate (cAMP) levels were detected to determine the level of translocation of RSp0213-CyaA' protein in tobacco leaves for each strain. Four independent biological replicates were made.

a good control for the whole process, from the protein extraction protocol in the supernatants to the statistical analysis of the MS detection.

RipBJ, a New *R. solanacearum* Type 3 Effector—The global comparison of the GMI1000 wild-type secretome with the *hrcV* mutant secretome by LC MS/MS allowed us to highlight proteins specifically secreted by the T3SS (Fig. 2B). We noticed that the RSp0213 hypothetical protein clustered within the T3-proteins in the PCA (Fig. 2B) and RSp0213 appeared to be differentially secreted between both strains, with a p value = $1.50 \cdot 10^{-5}$ (Fig. 2C; supplemental Table S2). In order to test the hypothesis that RSp0213 encodes a previously overlooked Rip effector protein, we performed *in vitro* secretion assay using GMI1000 and *hrcV* mutant strains expressing an RSp0213-HA fusion construct. Immunoblotting using an anti-HA antibody revealed that RSp0213-HA fusion proteins were present in both strains, but the RSp0213-HA secretion was only detected from the wild-type strain (Fig. 3A). To definitely show that RSp0213 is a *bona fide* Rip T3E, we performed a translocation assay based on the adenylate cyclase reporter system (40). GMI1000 and *hrcV* mutant strains carrying RSp0213-CyaA' fusion constructs were generated, and infiltrated in tobacco leaves. Seven hours after infiltration,

tobacco leaves were harvested and cAMP levels were measured using cAMP Biotrak competitive enzyme immunoassay (37). High amounts of cAMP were detected for the wild-type strain but not for the *hrcV* T3-defective mutant, indicating that RSp0213 was translocated into plant cells through the T3SS (Fig. 3B). These experiments showed that RSp0213 encodes a T3E, which was therefore renamed RipBJ following the proposed nomenclature for *R. solanacearum* T3Es (11). A *ripBJ* disruption mutant was generated and used to evaluate the contribution of this effector to pathogenicity on *A. thaliana* and *M. truncatula*, and to hypersensitive response (HR) elicitation after infiltration of tobacco leaves. No differences could be observed between the *ripBJ* mutant and the wild-type strain for none of these bioassays (supplemental Fig. S5).

Insights into Type 3 Secretion Regulation from the Secretome Analysis of *hrp*-Associated Mutants—The comparative secretome analysis between the wild-type strain and a *hrp* deficient mutant showed that our analysis enables the fine characterization of T3-secretome, but also allows for the comparative quantification of detected proteins between strains. The sensitivity of the method incited us to explore and compare the secretomes of potential T3S regulators. Some of them were characterized in phytopathogenic bacteria for their participation to T3E delivery, by promoting or repressing secretion through protein–protein interactions (21, 23). In *R. solanacearum* strain GMI1000, four potential Hpa proteins were identified: HpaB (RSp0853), HpaD (RSp0848), HpaG (RSp0842), and HpaP (RSp0862). *Hpa* genes are *hrpB*-regulated (41), physically associated to the *hrp*-cluster and not secreted. HpaB and HpaD have features of molecular chaperones (20, 42) with small sizes (16.8 kDa and 13.9 kDa, respectively) and acidic pI (4.4 and 4.2, respectively). HpaP was recently shown to modulate T3S (23) and HpaG (also known as LrpE) is a leucine-rich repeats (LRR) containing protein that negatively regulates the production of Hrp pili (43). We conducted secretome analyses of the *hpaB*, *hpaD*, and *hpaG* mutants using a similar experimental procedure as described above (supplemental Fig. S2C). We detected 260, 279, and 262 proteins in the secretomes of the *hpaB*, *hpaD*, and *hpaG* mutants, respectively (supplemental Table S3; supplemental Fig. S3). The first two components of the PCA conducted on the secreted proteins detected in the five strains (wild-type, *hrcV* and *hpa* mutants) clearly identified the strain effect, discriminating all strains and particularly singling out the *hrcV* mutant (Fig. 4A). The proteins responsible for this sample distribution are highlighted on Fig. 4B. Group 1 contains the RipF1 translocon proteins (44) and RipAB (formerly named PopB) (18). Group 2 consists of the HrpY pilin and the harpins RipX and RipW (formerly PopA and PopW) (45, 46). Group 3 contains RipC1, RipD, RipG7, RipM, and RipAC, which are among the most abundant T3Es in the wild-type strain supernatant (see supplemental Table S1). Group 4 contains proteins with a lower secretion level in the wild-type strain (supplemental Table S1) but with a high discriminating

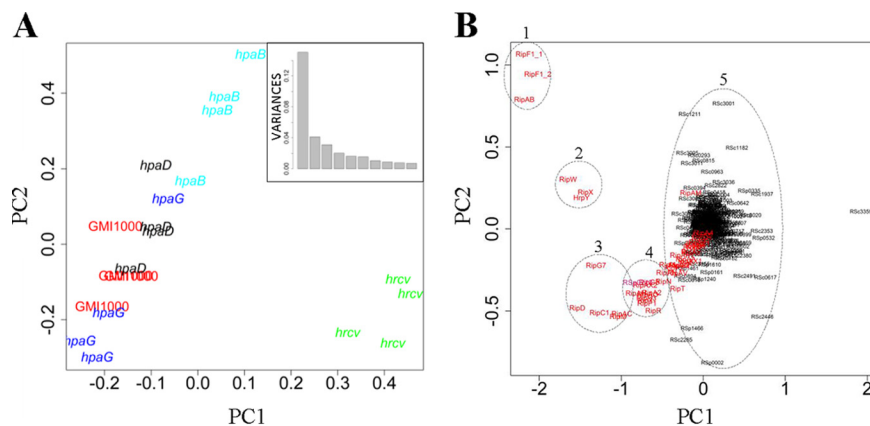


FIG. 4. *R. solanacearum* LC-MS/MS secretomes of T3-mutants highlight specific secretion patterns for each mutant. A, PCA with all the secreted proteins in the wild-type strain, in the *hrcV* mutant and in three *hpa* mutants highlights the strain effect on the first component, which represents a standard deviation of 0.39 and explains 44% of the total variance (box). B, Same PCA as in A shows that main discriminating proteins belong to T3-associated proteins (in red) and different protein groups may be identified (dotted line circles).

value upon the *glht* post-hoc test (supplemental Table S2), whereas group 5 corresponds to the bulk of the remaining proteins. PCA performed on the five strain secretomes, excluding T3-associated proteins, shows no highly discriminating component (supplemental Fig. S6).

To more accurately evaluate the role of the *hpa* genes in T3S, we compared the detected T3-proteins in the wild-type strain versus each *hpa* mutant using a *glht* post-hoc test (Fig. 5; supplemental Table S3). The *hpaB* mutant shows three classes of secretion patterns: (1) a class of proteins with a high level of secretion, but mainly not differentially secreted as compared with GMI1000, which corresponds to HrpY, RipF1, and RipAB proteins, along with the RipW and RipX harpins; (2) a class of 25 proteins with a reduced level of secretion in the *hpaB* mutant; and (3) a class of five effectors with a low level of detection, which are not detected in the *hpaB* mutant (Fig. 5A). The *hpaB* mutant appears therefore strongly altered in its secretion of effectors but not of the components of the T3SS machinery. The *hpaD* mutant shows a secretion pattern close to the wild-type strain, with only four Rip significantly differentially detected (Fig. 5B). In contrast, the *hpaG* mutant secretome reveals a global over-secretion pattern. Indeed, even if few Rips are differently secreted in the mutant compared with the wild-type (RipAB, RipF1_1, RipF1_2, and RipR), we can observe that numerous Rips are more secreted by the *hpaG* mutant than the wild-type (Fig. 5C). Six Rips were detected only in the *hpaG* mutant (RipV1, RipAK, RipAS, RipA4, RipAR, and RipAZ1).

Three Main Classes of Type 3 Effectors Based on Secretion Pattern Specificities—We used the log-normalized PAI data to perform a double hierarchical clustering in order to classify both the secreted Rips and the bacterial samples, according to the secretion of those Rip proteins. This analysis revealed two main groups of strains: *hrcV* and *hpaB* mutants on one hand, and *hpaD*, *hpaG* mutants, and GMI1000 on the other hand (Fig. 6). The separation of these two groups is caused by

the differences in the quantification of 17 proteins from group “a” (including the newly identified RipBJ (RSp213). These proteins are more abundant in the GMI1000/*hpaD*/*hpaG* secretomes than in the *hpaB*/*hrcV* ones. Likewise, the “b” group differentiates the *hrcV* from the other strains on the study, because of the absence of the Hrp pilus component and of the harpins in the *hrcV* mutant, thus revealing that regulation of RipAB and RipAM secretion is tightly linked at the post translational level. The “c” group corresponds to the six Rips only detected in the *hpaG* mutant secretome. The “d” subgroup clustered the 15 remaining Rips, which are also quantified in higher amount in the *hpaG* mutant.

In order to validate these specific secretion patterns obtained by MS, secretion assays were performed on several effectors showing (according to Fig. 2C) either high levels of secretion (RipAB, RipW, RipD, RipX, and RipG7), intermediate levels of secretion (RipH3, RipP1, RipAN, and RipP2), weak levels of secretion (RipAA, RipAV, and RipH2), or not detected by MS (RipH1). The abundance of these selected proteins was determined by immunoblotting protein extracts of cell pellets and of culture supernatants produced in the same conditions as the MS samples. In pellets, all the Rips were produced by the different strains in equal amount, except for *hpaG* mutant, as a slight overproduction can be observed for some Rips (Fig. 7). In supernatants, a different pattern of secretion can be observed: RipW, RipX, and RipAB were secreted in equal quantity by the three *hpa* mutants when compared with the wild-type strain (Fig. 7A). Combining MS data and Western blot experiments confirmed that the harpins RipW and RipX, as well as RipAB, share a similar secretion pattern. These Rips are thus secreted (in high amounts) independently of the three Hpa proteins. In Fig. 7B, we can observe that RipG7 is equally secreted in the *hpaD* and *hpaG* mutants compared with the wild-type, and less secreted in the *hpaB* mutant. This reflects the partial involvement of HpaB for strongly secreted Rips. Fig. 7C and 7D show the proteins

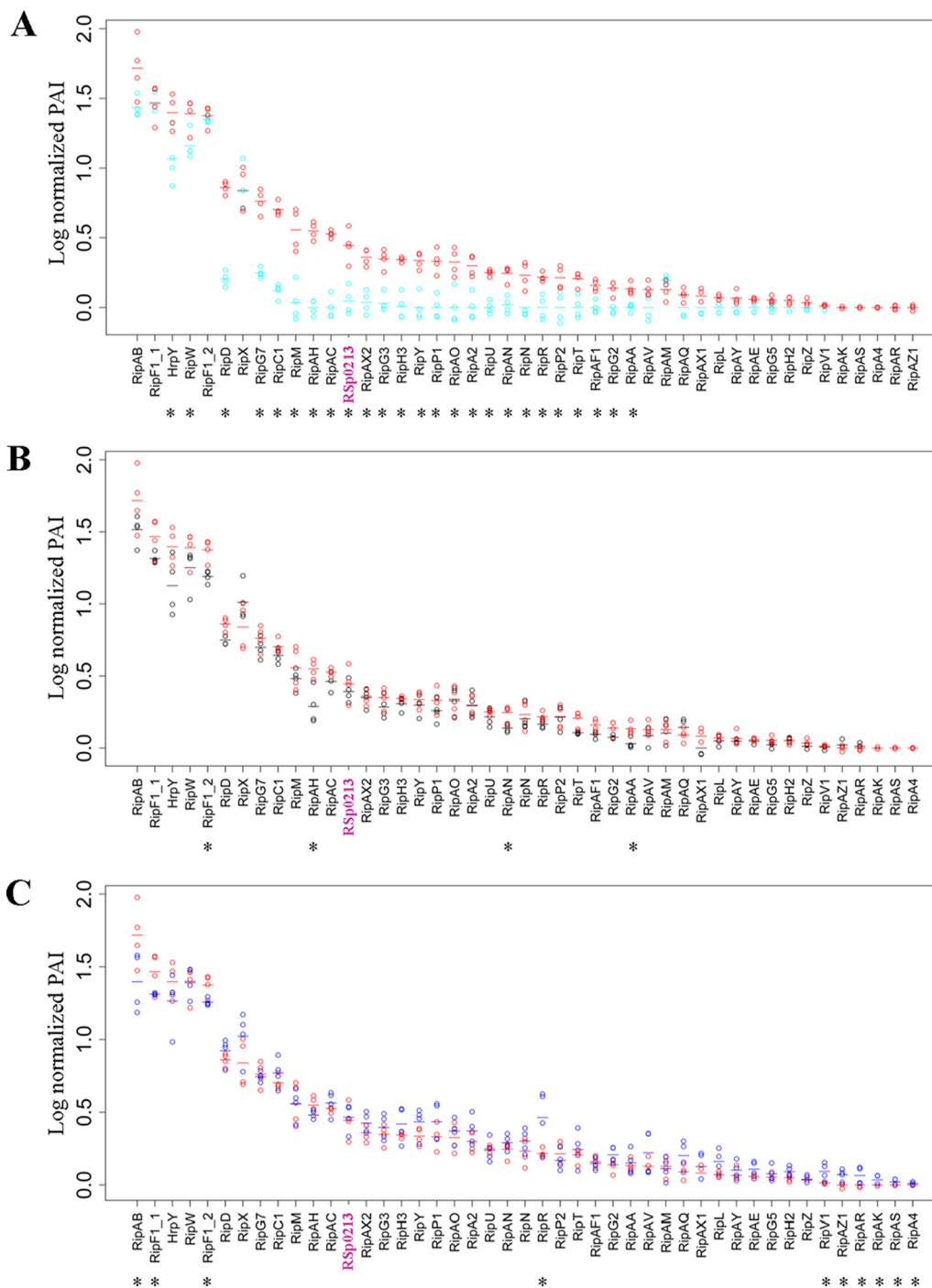


FIG. 5. Log-normalized PAI values of T3-associated proteins detected in the secretomes of the wild-type (red) and of *hpa* mutants show different T3S patterns. A, *hpaB* mutant in cyan. B, *hpaD* mutant in black. C, *hpaG* mutant in blue. Four biological replicates were analyzed for each bacterial strain. Each dot represents a replicate; dashes represent the mean value for all four replicates. The proteins were classified according to their level of secretion in the wild-type strain (from the strongest to the lowest log-normalized PAI detection). Asterisks highlight proteins presenting significantly different secretion levels between strains (glht post-hoc test, p value < 0.05).

(RipH3, RipP1, RipP2, RipAA, RipD, RipH2, RipAN, and RipAV) that are not secreted by *hrcV* nor *hpaB* mutants. This data confirms the secretion patterns observed by MS and highlights the specific requirement of *hpaB* for their secretion. Additionally, we observe an increased secretion for all these

proteins in the *hpaG* mutant, which also validate the original over-secreting MS pattern of this mutant (Fig. 5C). We can notice that this over-secretion can be independent (Fig. 7C) or not (Fig. 7D) of an over-production of these proteins in the *hpaG* mutant. This reflects the involvement of HpaG in the

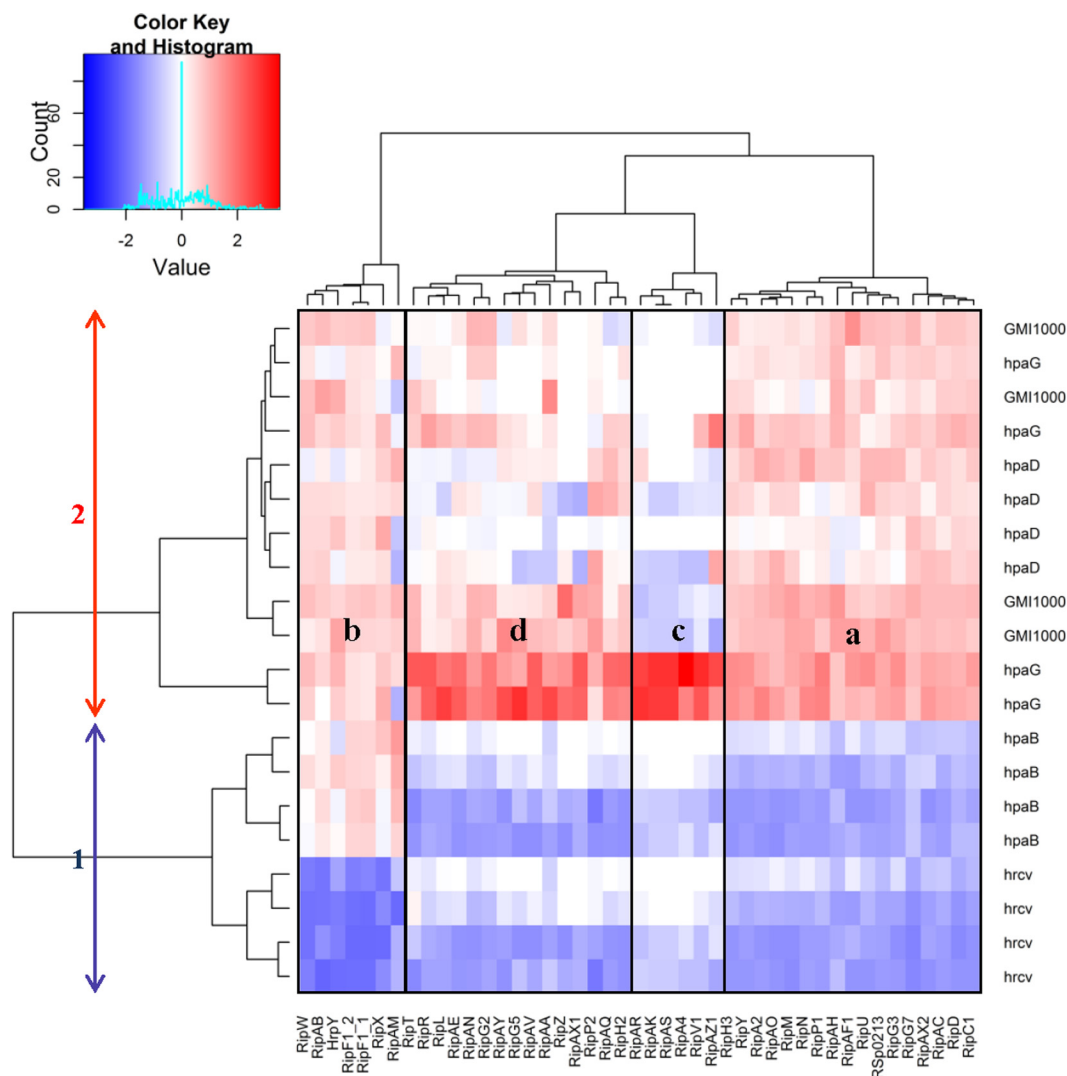


FIG. 6. **Double hierarchical clustering of bacterial strains and T3-proteins.** Bacterial strains thus produced two main clusters (arrows). Different protein subgroups according to their secretion patterns could be identified (a to d). White color represents a Z-score of 0 whereas red and blue shades represent higher and lower log-normalized PAI values, respectively.

control of T3E synthesis, but also potentially in transcriptional regulations or in protein stabilization. Finally, Fig. 7E shows that Western blot detection is more sensitive than MS detection as we can observe an *hpaB*-dependent pattern of secretion for RipH1, not detected in our MS analysis. However, the immunoblot analyses confirmed the specific patterns observed with MS analysis.

The Abundances of the Detected Effectors in the Bacterial Supernatants and That of Their Corresponding Gene Transcripts are Positively Correlated—In order to identify critical parameters determining the MS detection threshold, we investigated whether MS detection of the 44 secreted Rip effectors could be correlated either with structural features such as the isoelectric point (pI) or molecular weight (MW), or with transcription levels (as deduced from RNA sequencing approaches) (supplemental Fig. S7). The pI values of the detected Rips ranges from 4.2 (RipX) to 11.8 (RipAO), displaying

a homogenous distribution between all the ranges of pI (supplemental Fig. S7A and S7B). The MW of the Rips ranges from 10 kDa (RipAG and RipAH) to 278 kDa (RipS4), with half of the Rips between 20 kDa to 80 kDa. The distributions observed in supplemental S7C and S7D could not clearly attribute a lower or higher detection rate according to the MW, since this detection ranged from RipAH (10 kDa) to RipR (186 kDa). However, the RipA and RipS protein families (formerly named AWR and SKWP families, respectively) having the highest molecular weight among *R. solanacearum* T3Es were less efficiently detected. Indeed, among the five paralogs of the RipA family (ranging from 113 kDa to 141 kDa), only RipA2 is detected and none of the six RipS paralogs (>250 kDa, except for RipS6) could be detected (Fig. 2; see supplemental Table S4 for exhaustive pI and MW Rip data). We also looked for a possible correlation between RNA abundance (RNA-Seq data) and MS detection. This was done by taking advantage

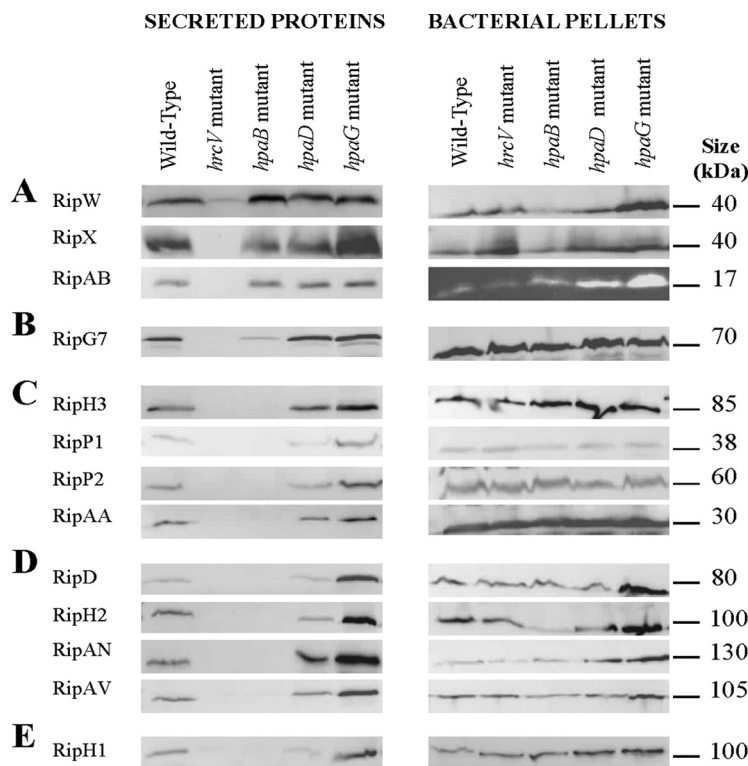


FIG. 7. Western blot validations of Rip secretion patterns. Secretion assays were performed in T3-inducing conditions, for the GMI1000 wild-type strain, and the *hrcV*, *hpaB*, *hpaD*, and *hpaG* mutants. Total proteins from bacterial pellets and supernatants were analyzed by Western-blot. Two to three biological replicates were done for each set of five strains.

of RNA-Seq experiments performed in the same inducing medium (Guidot *et al.*, in preparation). We observed a positive correlation between the *Rip* RNA abundance and the cognate protein detection in the supernatant (supplemental Fig. S7E and S7F). We fitted a linear model to explain the log-normalized PAI values by the squared rpkms values from the RNA-Seq dataset. We obtained the following formula $\log(\text{normalized PAI}) = 0.1509 + 0.0093 \cdot \text{rpkms}^2$ where the *p* values for intercept (0.1509) and slope (0.0093) are 0.07 and 6.10^{-4} , respectively (supplemental Fig. S7G). Therefore, except for the RipA and RipS family which correspond to very large proteins, no apparent differences could be attributed between detected and not-detected Rips in term of pl or MW, the threshold of Rip detection being very probably dependent on gene transcription, and thus to the amount of intracellular proteins produced.

Altered Secretion of Rip Proteins in the *hpaB* and *hpaG* Mutants is Associated with Impaired Virulence on *M. truncatula*—We then wanted to evaluate the impact of these modulations of Rip secretion on *R. solanacearum* pathogenicity on several host plants. We first validated that the *hpaB*, *hpaD*, and *hpaG* mutants were not affected in their growth in complete or minimal medium (data not shown). The three *hpa* mutant strains were leaf-infiltrated on *N. tabacum*, and root-inoculated on *A. thaliana* and *M. truncatula*. The *hpaD* mutant triggered an HR similar to the wild-type strain on tobacco plants, and virulence on *A. thaliana* and *M. truncatula* plants were undistinguishable from the wild-type strain (supplemental Fig. S8). The *hpaB* mutant was strongly affected in path-

ogenicity (Fig. 8). Indeed, the *hpaB* mutant is no more able to trigger an HR on tobacco, a phenotype complemented by the wild-type *hpaB* allele (Fig. 8A). The *hpaB* mutant was also unable to induce disease on *A. thaliana* (Figs. 8B and 9C), or on *M. truncatula* (Fig. 8D). Finally, HpaG was found to be dispensable for HR induction on tobacco (supplemental Fig. S8A) as well as for *R. solanacearum* pathogenicity on *A. thaliana* (Fig. 9A). However, disease development was delayed and significantly reduced on *M. truncatula* compared with the wild-type strain (Fig. 9B and 9C). *M. truncatula in planta* bacterial growth showed that HpaG is also required for bacterial multiplication, with a decrease of more than 100-fold for the *hpaG* mutant compared with the wild-type strain. Bacterial multiplication was restored in the *hpaG*-complemented strain (Fig. 9C).

DISCUSSION

Phytopathogenic bacteria have evolved multiple strategies to infect plants. A major determinant of bacterial pathogenicity is the T3SS that delivers effector proteins directly into the host cells. Despite increasing knowledge on the control of the T3SS through transcriptional regulatory networks, only limited information on post-translational regulations is available. This study provides the first characterization of the T3-dependent secretome of *R. solanacearum* using the recent and advanced Q Exactive technology. To date, some T3-secretomes of animal pathogenic bacteria have been characterized (47–49), but only partial secretome and proteome analyses are available from plant pathogenic bacteria since these studies

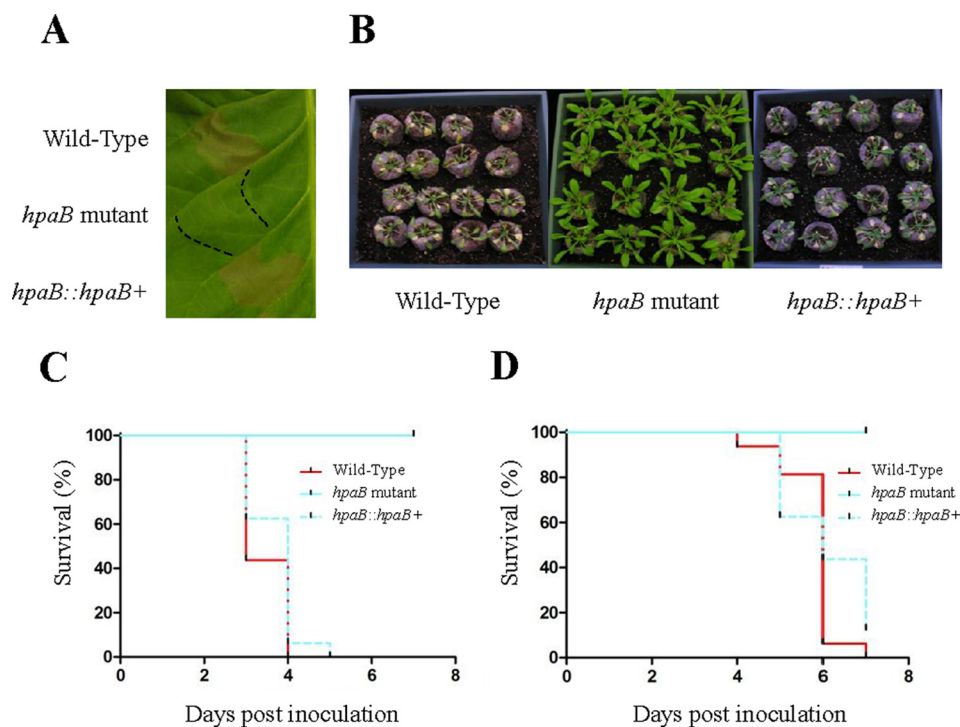


FIG. 8. HpaB is required to induce HR on tobacco and disease on *A. thaliana* and *M. truncatula*. A, GMI1000 wild-type strain, *hpaB* mutant and complemented *hpaB* mutant inoculated on *N. tabacum*. HR is observed only with GMI1000 and with the complemented *hpaB* mutant 24 h after leaf infiltration. B, pictures of *A. thaliana* Col-0 plants 6 days post inoculation. C, Kaplan-Meier survival analysis of 16 *A. thaliana* inoculated plants. Gehan-Breslow-Wilcoxon test indicates that the wild-type strain curve (red) is significantly different from the *hpaB* mutant curve (cyan) (p value < 0.001), contrary to the complemented *hpaB* curve (dotted cyan) (p value = 0.8702). D, Kaplan-Meier survival analysis of 16 *M. truncatula* inoculated plants. Gehan-Breslow-Wilcoxon test indicates that the wild-type strain curve (red) is significantly different from the *hpaB* curve (cyan) (p value < 0.001), contrary to the complemented *hpaB* curve (dotted cyan) (p value = 0.5416). All these experiments were repeated at least three times.

mainly used two-dimensional gel electrophoresis followed by MALDI-TOF-MS or nano-LC-MS/MS approaches (50–55). With a total of 228 proteins detected in the wild-type strain supernatant (supplemental Table S1), this study therefore represents the most exhaustive secretome inventory to date among bacterial plant pathogens. In addition, the analysis of *hpa* mutants revealed specific T3-secretome patterns, showing both the sensitivity of the methodology and its efficiency to decrypt T3-secretomes and to describe the impact of T3-post-translational regulators in the secretion process. Combining the data obtained for the four biological replicates of the five strains analyzed in this study, we could detect 320 secreted proteins. Among them, 66% were predicted to be secreted using SecretomeP 2.0 (<http://www.cbs.dtu.dk/services/SecretomeP/>), SignalP 4.0 (<http://www.cbs.dtu.dk/services/SignalP-4.0/>), and MaGe (Magnifying Genomes Microbial Genome Annotation System) (<http://www.genoscope.cns.fr/agc/microscope/mage/index.php>). We also showed with Western blot experiments that the non-detection of some Rips using MS is not because of a non-secretion in our experimental conditions, but is because of the MS detection threshold. Detection of 60% of the *R. solanacearum* GMI1000 known effectors (43 out of 72 (11)) is satisfactory compared with other T3-secretome studies (51–55) and considering that

several Rip effectors may certainly be low-abundant proteins produced at the host cell contact. We observed a direct correlation between *rip* gene transcription and the quantitative detection of the corresponding proteins through MS analysis. Quantitative MS data were also supported by Western blot experiments. Absence or residual spectral counting for Rips in the *hrcV* mutant was confirmed by the absence of detection of Rips in bacterial supernatants after immunoblot experiments whereas these proteins were well produced in the *hrcV* bacterial pellets. Contrary to all the other Rips tested, RipW was detected as slightly secreted by the *hrcV* mutant as shown by MS (Fig. 2C) or Western blot experiments (Fig. 7A). The contrasting secretion patterns of the *hpaB* and *hpaG* mutants, with specific proteins either less or more secreted than the wild-type, were also validated by specific immunodetections. All these observations confirm the overall quality and sensitivity (reproducibility of detection of differentially secreted proteins) of the MS experimental process we used.

Our study identified a novel effector, RipBJ, which contains an N-terminal sequence homologous to RipAG and RipAH, but also to AvrRpm1 and AvrPto *P. syringae* effectors (supplemental Fig. S5D). This N-terminal sequence domain contains putative myristoylation/acylation signals which were shown to be required for the targeting of AvrRpm1 to the

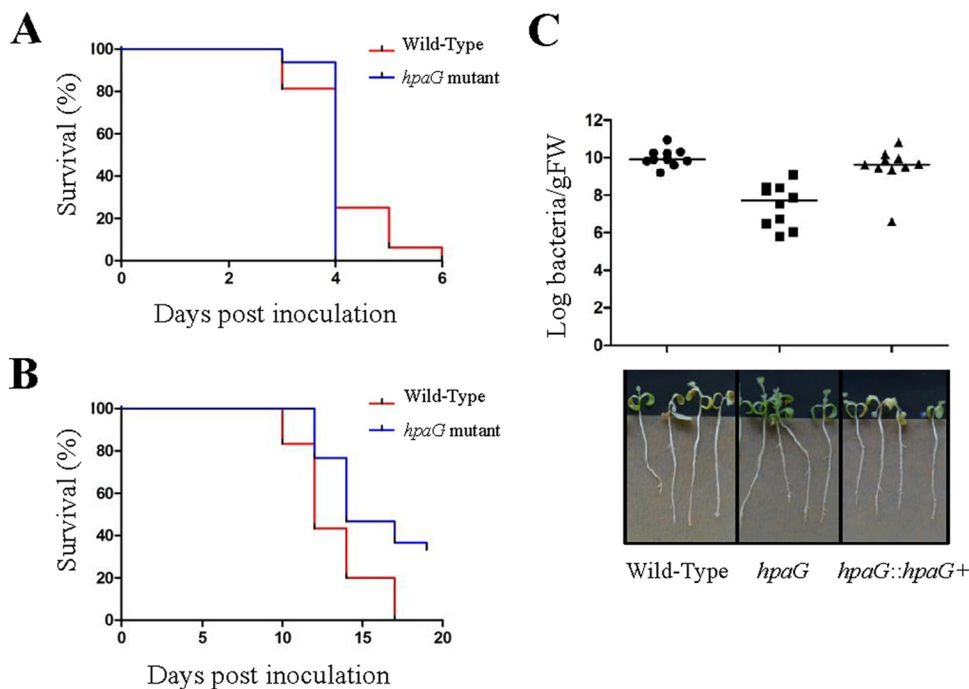


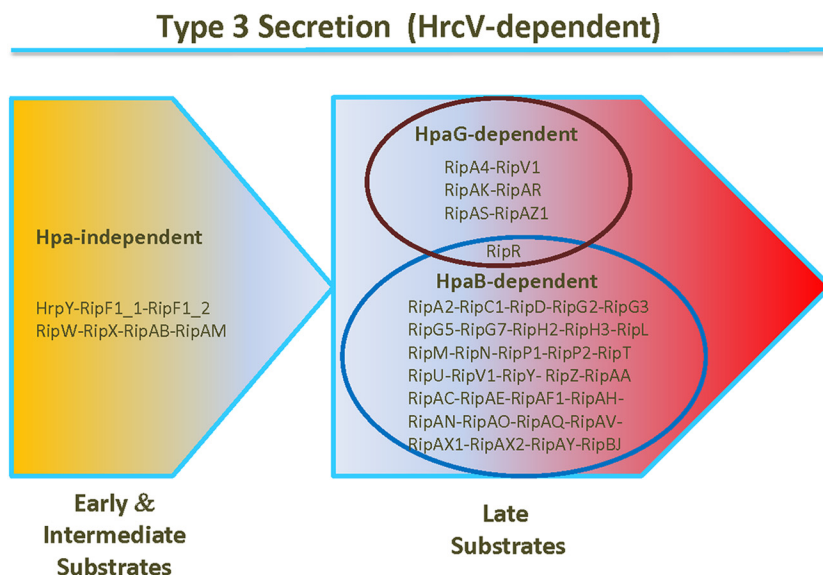
FIG. 9. *hpaG* mutant is strongly reduced in virulence on *M. truncatula*. A, Kaplan-Meier survival analysis of 16 *A. thaliana* plants inoculated with *R. solanacearum* wild-type strain (red) and *hpaG* mutant (blue). Gehan-Breslow-Wilcoxon test indicates that the two curves are not significantly different (p value = 0.4845). B, Kaplan-Meier survival analysis of 16 *M. truncatula* plants inoculated with *R. solanacearum* wild-type strain (red) and *hpaG* mutant (blue). Gehan-Breslow-Wilcoxon test indicates that the two curves are significantly different (p value = 0.002). Three biological replicates were performed (A–B). C, measurement of *in planta* bacterial growth using *in vitro* *M. truncatula* plants, 14 days post inoculation. Each dot represents a replicate of three plants, the black line specifies the median of the ten replicates. Mann-Whitney-Wilcoxon tests were performed and indicate that the *in planta* bacterial multiplication of the *hpaG* mutant is different from the wild-type strain (p value < 0.001), but not the complemented *hpaG* mutant (p value = 0.1655). Representative pictures were taken 17 days post inoculation.

plasma membrane (56). However, no difference could be observed between the wild-type strain and the *ripBJ* mutant in pathogenicity assays, probably because of functional redundancy among Rip effectors (15–17). In a former study (23), we provided evidence of a post-translational control of T3E secretion in *R. solanacearum* by the HpaP protein. In this work, we combined proteomic and phenotypic analyses studying three additional *hpa* mutants, *hpaB*, *hpaD*, and *hpaG*. Our work showed that these *hpa* mutants have three distinct secretion patterns, with specific proteomic signatures highlighting Rip classes of T3S.

hpaB mutant secretome analysis showed the strongest Rip secretory phenotype. Indeed, secretion of almost all the Rips detected in the wild-type strain supernatant was partly or fully altered in the *hpaB* mutant. This global defect in Rip secretion is likely to be the cause of the nonpathogenicity phenotype of the *hpaB* mutant. This corroborates previous works on *hpaB* homologs in several phytopathogenic bacteria. In another strain of *R. solanacearum*, HpaB was shown to be required for the translocation of at least 66 T3Es (57, 58). Studies in *Xanthomonas campestris* pv. *vesicatoria* (*Xcv*) showed that HpaB had a central role in *Xcv* efficient T3S, notably interacting with various control proteins and T3Es (6, 22). HpaB homologs were shown to be required in bacterial pathogenicity but with different specificities according to the pathosys-

tems studied (57, 59, 60). In our study, we show that the *hpaB* mutant is still capable of secreting HrpY, furthermore there is also efficient secretion of RipX and RipW harpins (45, 46), altogether suggesting that the Hrp pilus is functional in this mutant. Interestingly, RipAB appears to be the most abundantly secreted Rip, and is still efficiently secreted in the *hpaB* mutant. Additionally, the hierarchical clustering obtained taking into account the five strains clustered the HrpY pilin, the RipF1_1 and RipF1_2 translocators, the RipX and RipW harpins with RipAB and RipAM. The RipF1 paralogs are required for efficient Rip translocation (11), but a direct interaction between RipF1_1 and HrpY could not be identified (44). Even if RipAM has a lower secretion level compared with the other proteins of this group, similar pattern is observed. All together, these data led us to hypothesize that RipX, RipW, RipAB, and RipAM could be involved, in an Hpa protein-independent manner, in the first stages of Rip translocation process. This hypothesis is in accordance with a polymutant approach in Pst DC3000 which highlighted a consortium of redundant translocators required to promote Pst T3E injection into plant cells (61, 62). RipF1, RipW, RipX, RipAB, and RipAM all belong to the *R. solanacearum* core effectome (11). It will be of particular interest to study more precisely how they take part in the formation of the Hrp translocation apparatus as acces-

FIG. 10. Involvement of Hpa proteins in Rip secretion. This illustration proposes subsets of Rips for which T3S is coregulated, in an Hpa-independent or Hpa-dependent way. The model is based on the T3-specific secretion patterns of the GMI1000 wild-type strain and of the *hpa* mutants. Data obtained from the statistical analysis on MS assays, from the following hierarchical clustering, and from the Western blot validation experiments were combined. The two groups represent “early/intermediate” and “late” substrates of T3SS, respectively. Among the late substrates, the blue circle contains the Rips whose secretion is positively regulated by HpaB, whereas the red circle contains the Rips whose secretion is negatively regulated by HpaG.



sory cotranslocators, notably by looking for interactions between them and the HrpY pilin.

The *hpaG* mutant secretome analysis showed a deregulation of the *hrp*-secretion with an unexpected MS-over-secretion pattern, numerous Rips being more detected compared with the wild-type strain. Although still able to induce an HR on tobacco plants and the full disease on *A. thaliana*, the *hpaG* mutant is specifically impaired in its pathogenicity on *M. truncatula*. In addition, RipG7, which is strictly required for *R. solanacearum* pathogenicity on *M. truncatula* (17), is still efficiently secreted by the *hpaG* mutant. A study with another strain of *R. solanacearum* on a HpaG homolog protein (LrpE) showed a slight virulence reduction of the *lrpE* mutant on eggplant (43). Thus, we hypothesize that these host phenotypes depend more on altered secretion of some effectors directly involved on certain hosts to confer disease. One or several Rips could be directly involved in this phenotype on the model legume plant, letting us hypothesize a potential HpaG function as a secretion suppressor of Rips involved in the induction of plant immunity. We also observed that over-secretion of Rips by the *hpaG* mutant can also be associated with specific over-production of Rips, suggesting a role for HpaG in transcriptional control or on protein stabilization for a subset of Rips.

This article constitutes another piece of the puzzle of T3S post-translational control, and even if many questions remain, this first *R. solanacearum* secretome study supports the existence of a T3S hierarchy with specific subsets of effectors having differential secretion patterns (Fig. 10). The study of three *hpa* mutants revealed previously unknown complex regulations of T3S, and Rips with similar regulation profiles. This work also showed that HpaB and HpaG proteins are post-translational regulators of T3S, with opposite roles on T3S. Indeed, although there is no evidence for a role of HpaD in T3S post-translational control, HpaB clearly promotes secre-

tion of numerous Rips and acts as a positive regulator of T3S, whereas HpaG seems to negatively regulate secretion of other Rips. A recent review on orchestration of T3S from animal and plant pathogenic bacteria classified the pilus as an “early” T3S substrate, translocon proteins as “intermediate” substrates and effector proteins as “late” substrates (6). Here, we identified a first set of Rips whose secretion is Hpa-independent which we propose to qualify as putative “early/intermediate” substrates as they include secreted syringe components HrpY and RipF1 proteins. We highlighted a second set of Rips whose secretion is Hpa-dependent, which we hypothesize as putative “late” substrates, with either a strict, or a quantitative Hpa-secretion control. This also suggests a sequential secretion in *R. solanacearum*, between “early/intermediate” and “late” substrates, helping to define new subsets of Rips under secretion process (Fig. 10). This work illustrates how the Rip secretion is finely tuned and how this control can impact host specificity. We showed that we were able to monitor secretion of more than 40 Rips per assay. A polymutant approach could help to identify T3Es collectively involved on different host plants.

Acknowledgments—We thank Jean Luc Pariente and Claudette Icher for tobacco plant preparation. We thank Elise Gay for technical assistance for construction of strains with effector-HA tag, and Lenaïck Belliot for LBy5 and LBy14 plasmids. We thank Alice Guidot and Laure Plener for generously providing transcription data of *Rip* genes. We thank Laurent Deslandes for the gift of the PopP2 antibody. We thank Anne Aubert Frambourg and Michel Zivy for fruitful discussions.

* This work was supported by a French Agence Nationale de la Recherche grant (ANR-2010-JCJC-1710-01) to F.V. This work benefited from interactions promoted by COST Action FA 1208 <https://www.cost-sustain.org>. Our work is performed at the Laboratoire des Interactions Plantes-Microorganismes that is part of the Laboratoire d'Excellence (LABEX) entitled TULIP (ANR-10-LABX-41). F.L and D.L. were funded by a grant from the French Ministry of National Education and Research.

 This article contains supplemental Procedures, Figs. S1 to S8, and Tables S1 to S4.

** To whom correspondence should be addressed: Unité Mixte de Recherche 2594/441, Centre National de Recherche Scientifique (CNRS)/Institut National de Recherche Agronomique, Laboratoire des Interactions Plantes-Microorganismes, 24 Chemin de Borde Rouge-Auveville CS 52627, Castanet-Tolosan 31326 France. Tel.: +33 (0)5 61 28 57 76; E-mail: fabienne.vaillau@toulouse.inra.fr.

REFERENCES

1. Mansfield, J., Genin, S., Magori, S., Citovsky, V., Sriariyanum, M., Ronald, P., Dow, M., Verdier, V., Beer, S. V., Machado, M. A., Toth, I., Salmond, G., and Foster, G. D. (2012) Top 10 plant pathogenic bacteria in molecular plant pathology. *Mol. Plant Pathol.* **13**, 614–629
2. Hayward, A. C. (1991) Biology and epidemiology of bacterial wilt caused by *Pseudomonas solanacearum*. *Annu. Rev. Phytopathol.* **29**, 65–87
3. Genin, S. (2010) Molecular traits controlling host range and adaptation to plants in *Ralstonia solanacearum*. *New Phytol.* **187**, 920–928
4. Tampakaki, A. P., Skandalis, N., Gazi, A. D., Bastaki, M. N., Sarris, P. F., Charova, S. N., Kokkinidis, M., and Panopoulos, N. J. (2010) Playing the “Harp”: evolution of our understanding of hrp/hrc genes. *Annu. Rev. Phytopathol.* **48**, 347–370
5. Büttner, D., and He, S. Y. (2009) Type III protein secretion in plant pathogenic bacteria. *Plant Physiol.* **150**, 1656–1664
6. Büttner, D. (2012) Protein export according to schedule: architecture, assembly, and regulation of type III secretion systems from plant- and animal-pathogenic bacteria. *Microbiol. Mol. Biol. Rev.* **76**, 262–310
7. Petnicki-Ocwieja, T., Schneider, D. J., Tam, V. C., Chancey, S. T., Shan, L., Jamir, Y., Schechter, L. M., Janes, M. D., Buell, C. R., Tang, X., Collmer, A., and Alfano, J. R. (2002) Genomewide identification of proteins secreted by the Hrp type III protein secretion system of *Pseudomonas syringae* pv. tomato DC3000. *Proc. Natl. Acad. Sci. U.S.A.* **99**, 7652–7657
8. Salanoubat, M., Genin, S., Artiguenave, F., Gouzy, J., Mangenot, S., Arlat, M., Billault, A., Brottier, P., Camus, J. C., Cattolico, L., Chandler, M., Choisine, N., Claudel-Renard, C., Cunnac, S., Demange, N., Gaspin, C., Lavie, M., Moisan, A., Robert, C., Saurin, W., Schiex, T., Siguier, P., Thebault, P., Whalen, M., Wincker, P., Levy, M., Weissenbach, J., and Boucher, C. A. (2002) Genome sequence of the plant pathogen *Ralstonia solanacearum*. *Nature* **415**, 497–502
9. Oh, C.-S., and Beer, S. V. (2005) Molecular genetics of *Erwinia amylovora* involved in the development of fire blight. *FEMS Microbiol. Lett.* **253**, 185–192
10. Thieme, F., Koebnik, R., Bekel, T., Berger, C., Boch, J., Büttner, D., Caldana, C., Gaigalat, L., Goesmann, A., Kay, S., Kirchner, O., Lanz, C., Linke, B., McHardy, A. C., Meyer, F., Mittenhuber, G., Nies, D. H., Niesbach-Klößgen, U., Patschkowski, T., Rückert, C., Rupp, O., Schneiker, S., Schuster, S. C., Vorhölter, F.-J., Weber, E., Pühler, A., Bonas, U., Bartels, D., and Kaiser, O. (2005) Insights into genome plasticity and pathogenicity of the plant pathogenic bacterium *Xanthomonas campestris* pv. *vesicatoria* revealed by the complete genome sequence. *J. Bacteriol.* **187**, 7254–7266
11. Peeters, N., Carrère, S., Anisimova, M., Plener, L., Cazalé, A.-C., and Genin, S. (2013) Repertoire, unified nomenclature and evolution of the Type III effector gene set in the *Ralstonia solanacearum* species complex. *BMC Genomics* **14**, 859
12. Cunnac, S., Boucher, C., and Genin, S. (2004) Characterization of the cis-acting regulatory element controlling HrpB-mediated activation of the type III secretion system and effector genes in *Ralstonia solanacearum*. *J. Bacteriol.* **186**, 2309–2318
13. Genin, S., and Denny, T. P. (2012) Pathogenomics of the *Ralstonia solanacearum* species complex. *Annu. Rev. Phytopathol.* **50**, 67–89
14. Remigi, P., Anisimova, M., Guidot, A., Genin, S., and Peeters, N. (2011) Functional diversification of the GALA type III effector family contributes to *Ralstonia solanacearum* adaptation on different plant hosts. *New Phytol.* **192**, 976–987
15. Solé, M., Popa, C., Mith, O., Sohn, K. H., Jones, J. D. G., Deslandes, L., and Valls, M. (2012) The *avr* gene family encodes a novel class of *Ralstonia solanacearum* type III effectors displaying virulence and avirulence activities. *Mol. Plant-Microbe Interact.* **25**, 941–953

16. Chen, L., Shiota, M., Zhang, Y., Kiba, A., Hikichi, Y., and Ohnishi, K. (2013) Involvement of HLK effectors in *Ralstonia solanacearum* disease development in tomato. *J. Gen. Plant Pathol.* **80**, 79–84
17. Angot, A., Peeters, N., Lechner, E., Vaillau, F., Baud, C., Gentzittel, L., Sartorel, E., Genschik, P., Boucher, C., and Genin, S. (2006) *Ralstonia solanacearum* requires F-box-like domain-containing type III effectors to promote disease on several host plants. *Proc. Natl. Acad. Sci. U.S.A.* **103**, 14620–14625
18. Guéron, M., Timmers, A. C., Boucher, C., and Arlat, M. (2000) Two novel proteins, PopB, which has functional nuclear localization signals, and PopC, which has a large leucine-rich repeat domain, are secreted through the hrp-secretion apparatus of *Ralstonia solanacearum*. *Mol. Microbiol.* **36**, 261–277
19. Feldman, M. F., and Cornelis, G. R. (2003) The multitasking type III chaperones: all you can do with 15 kDa. *FEMS Microbiol. Lett.* **219**, 151–158
20. Parsot, C., Hamiaux, C., and Page, A. L. (2003) The various and varying roles of specific chaperones in type III secretion systems. *Curr. Opin. Microbiol.* **6**, 7–14
21. Büttner, D., and Bonas, U. (2006) Who comes first? How plant pathogenic bacteria orchestrate type III secretion. *Curr. Opin. Microbiol.* **9**, 193–200
22. Lohou, D., Lonjon, F., Genin, S., and Vaillau, F. (2013) Type III chaperones & Co in bacterial plant pathogens: a set of specialized bodyguards mediating effector delivery. *Front. Plant Sci.* **4**, 435
23. Lohou, D., Turner, M., Lonjon, F., Cazalé, A.-C., Peeters, N., Genin, S., and Vaillau, F. (2014) HpaP modulates type III effector secretion in *Ralstonia solanacearum* and harbors a substrate specificity switch domain essential for virulence. *Mol. Plant Pathol.* **15**, 601–614
24. Pirmoradian, M., Budamgunta, H., Chinglin, K., Zhang, B., Astorga-Wells, J., and Zubarev, R. A. (2013) Rapid and deep human proteome analysis by single-dimension shotgun proteomics. *Mol. Cell. Proteomics* **12**, 3330–3338
25. Poueymiro, M., Cunnac, S., Barberis, P., Deslandes, L., Peeters, N., Cazale-Noel, A.-C., Boucher, C., and Genin, S. (2009) Two type III secretion system effectors from *Ralstonia solanacearum* GM1000 determine host-range specificity on tobacco. *Mol. Plant-Microbe Interact.* **22**, 538–550
26. Prentki, P., and Krisch, H. M. (1984) *In vitro* insertional mutagenesis with a selectable DNA fragment. *Gene* **29**, 303–313
27. González, A., Plener, L., Restrepo, S., Boucher, C., and Genin, S. (2011) Detection and functional characterization of a large genomic deletion resulting in decreased pathogenicity in *Ralstonia solanacearum* race 3 biovar 2 strains. *Environ. Microbiol.* **13**, 3172–3185
28. Washburn, M. P., Wolters, D., and Yates, J. R. (2001) Large-scale analysis of the yeast proteome by multidimensional protein identification technology. *Nat. Biotechnol.* **19**, 242–247
29. Sadygov, R. G., Liu, H., and Yates, J. R. (2004) Statistical models for protein validation using tandem mass spectral data and protein amino acid sequence databases. *Anal. Chem.* **76**, 1664–1671
30. Gilchrist, A., Au, C. E., Hiding, J., Bell, A. W., Fernandez-Rodriguez, J., Lesimple, S., Nagaya, H., Roy, L., Gosline, S. J. C., Hallett, M., Paiement, J., Kearney, R. E., Nilsson, T., and Bergeron, J. J. M. (2006) Quantitative proteomics analysis of the secretory pathway. *Cell* **127**, 1265–1281
31. Rappsilber, J., and Mann, M. (2002) What does it mean to identify a protein in proteomics? *Trends Biochem. Sci.* **27**, 74–78
32. Hothorn, T., Bretz, F., and Westfall, P. (2008) Simultaneous inference in general parametric models. *Biom. J. Biom. Z.* **50**, 346–363
33. R Core Team (2014) *R: A language and environment for statistical computing*. R Foundation for Statistical Computing, Vienna, Austria. <http://www.R-project.org/>
34. Smyth, G. K. (2005) In *Bioinformatics and computational biology solutions using R and Bioconductor* Springer, NY, pp 397–420
35. Wilkinson, L. (2012) Exact and approximate area-proportional circular Venn and Euler diagrams. *IEEE Trans. Vis. Comput. Graph.* **18**, 321–331
36. Lavie, M., Shillington, E., Eguiluz, C., Grimsley, N., and Boucher, C. (2002) PopP1, a new member of the YopJ/AvrRxv family of type III effector proteins, acts as a host-specificity factor and modulates aggressiveness of *Ralstonia solanacearum*. *Mol. Plant-Microbe Interact.* **15**, 1058–1068
37. Cunnac, S., Occhialini, A., Barberis, P., Boucher, C., and Genin, S. (2004) Inventory and functional analysis of the large Hrp regulon in *Ralstonia solanacearum*: identification of novel effector proteins translocated to plant host cells through the type III secretion system. *Mol. Microbiol.* **53**, 115–128

38. Deslandes, L., Olivier, J., Peeters, N., Feng, D. X., Khounloham, M., Boucher, C., Somssich, I., Genin, S., and Marco, Y. (2003) Physical interaction between RRS1-R, a protein conferring resistance to bacterial wilt, and PopP2, a type III effector targeted to the plant nucleus. *Proc. Natl. Acad. Sci. U.S.A.* **100**, 8024–8029
39. Vaillau, F., Sartorel, E., Jardinaud, M.-F., Chardon, F., Genin, S., Huguet, T., Gentzbittel, L., and Petitprez, M. (2007) Characterization of the interaction between the bacterial wilt pathogen *Ralstonia solanacearum* and the model legume plant *Medicago truncatula*. *Mol. Plant-Microbe Interact.* **20**, 159–167
40. Sory, M. P., and Cornelis, G. R. (1994) Translocation of a hybrid YopE-adenylate cyclase from *Yersinia enterocolitica* into HeLa cells. *Mol. Microbiol.* **14**, 583–594
41. Occhialini, A., Cunnac, S., Reymond, N., Genin, S., and Boucher, C. (2005) Genome-wide analysis of gene expression in *Ralstonia solanacearum* reveals that the *hrpB* gene acts as a regulatory switch controlling multiple virulence pathways. *Mol. Plant-Microbe Interact.* **18**, 938–949
42. Thomas, N. A., Ma, I., Prasad, M. E., and Rafuse, C. (2012) Expanded roles for multicargo and class 1B effector chaperones in type III secretion. *J. Bacteriol.* **194**, 3767–3773
43. Murata, Y., Tamura, N., Nakaho, K., and Mukaihara, T. (2006) Mutations in the *IrpE* gene of *Ralstonia solanacearum* affects Hrp pili production and virulence. *Mol. Plant-Microbe Interact.* **19**, 884–895
44. Meyer, D., Cunnac, S., Guéron, M., Declercq, C., Van Gijsegem, F., Lauber, E., Boucher, C., and Arlat, M. (2006) PopF1 and PopF2, two proteins secreted by the type III protein secretion system of *Ralstonia solanacearum*, are translocators belonging to the HrpF/NopX family. *J. Bacteriol.* **188**, 4903–4917
45. Arlat, M., Van Gijsegem, F., Huet, J. C., Pernollet, J. C., and Boucher, C. A. (1994) PopA1, a protein which induces a hypersensitivity-like response on specific *Petunia* genotypes, is secreted via the Hrp pathway of *Pseudomonas solanacearum*. *EMBO J.* **13**, 543–553
46. Li, J.-G., Liu, H.-X., Cao, J., Chen, L.-F., Gu, C., Allen, C., and Guo, J.-H. (2010) PopW of *Ralstonia solanacearum*, a new two-domain harpin targeting the plant cell wall. *Mol. Plant Pathol.* **11**, 371–381
47. Deng, W., de Hoog, C. L., Yu, H. B., Li, Y., Croxen, M. A., Thomas, N. A., Puente, J. L., Foster, L. J., and Finlay, B. B. (2010) A comprehensive proteomic analysis of the type III secretome of *Citrobacter rodentium*. *J. Biol. Chem.* **285**, 6790–6800
48. Niemann, G. S., Brown, R. N., Gustin, J. K., Stufkens, A., Shaikh-Kidwai, A. S., Li, J., McDermott, J. E., Brewer, H. M., Schepmoes, A., Smith, R. D., Adkins, J. N., and Heffron, F. (2011) Discovery of novel secreted virulence factors from *Salmonella enterica* serovar Typhimurium by proteomic analysis of culture supernatants. *Infect. Immun.* **79**, 33–43
49. Deng, W., Yu, H. B., de Hoog, C. L., Stoyanov, N., Li, Y., Foster, L. J., and Finlay, B. B. (2012) Quantitative proteomic analysis of type III secretome of enteropathogenic *Escherichia coli* reveals an expanded effector repertoire for attaching/effacing bacterial pathogens. *Mol. Cell. Proteomics* **11**, 692–709
50. Kazemi-Pour, N., Condemine, G., and Hugouvieux-Cotte-Pattat, N. (2004) The secretome of the plant pathogenic bacterium *Erwinia chrysanthemi*. *Proteomics* **4**, 3177–3186
51. Nissinen, R. M., Ytterberg, A. J., Bogdanove, A. J., VAN Wijk, K. J., and Beer, S. V. (2007) Analyses of the secretomes of *Erwinia amylovora* and selected *hrp* mutants reveal novel type III secreted proteins and an effect of HrpJ on extracellular harpin levels. *Mol. Plant Pathol.* **8**, 55–67
52. Robin, G. P., Ortiz, E., Szurek, B., Brizard, J.-P., and Koebnik, R. (2014) Comparative proteomics reveal new HrpX-regulated proteins of *Xanthomonas oryzae* pv. *oryzae*. *J. Proteomics* **97**, 256–264
53. Wang, Y., Kim, S. G., Wu, J., Huh, H.-H., Lee, S.-J., Rakwal, R., Agrawal, G. K., Park, Z.-Y., Young Kang, K., and Kim, S. T. (2013) Secretome analysis of the rice bacterium *Xanthomonas oryzae* (Xoo) using *in vitro* and *in planta* systems. *Proteomics* **13**, 1901–1912
54. Haapalainen, M., Mosorin, H., Dorati, F., Wu, R.-F., Roine, E., Taira, S., Nissinen, R., Mattinen, L., Jackson, R., Pirhonen, M., and Lin, N.-C. (2012) Hcp2, a secreted protein of the phytopathogen *Pseudomonas syringae* pv. *tomato* DC3000, is required for fitness for competition against bacteria and yeasts. *J. Bacteriol.* **194**, 4810–4822
55. Schumacher, J., Waite, C. J., Bennett, M. H., Perez, M. F., Shethi, K., and Buck, M. (2014) Differential secretome analysis of *Pseudomonas syringae* pv. *tomato* using gel-free MS proteomics. *Front. Plant Sci.* **5**, 242
56. Nimchuk, Z., Marois, E., Kjemtrup, S., Leister, R. T., Katagiri, F., and Dangl, J. L. (2000) Eukaryotic fatty acylation drives plasma membrane targeting and enhances function of several type III effector proteins from *Pseudomonas syringae*. *Cell* **101**, 353–363
57. Mukaihara, T., Tamura, N., Murata, Y., and Iwabuchi, M. (2004) Genetic screening of Hrp type III-related pathogenicity genes controlled by the HrpB transcriptional activator in *Ralstonia solanacearum*. *Mol. Microbiol.* **54**, 863–875
58. Mukaihara, T., Tamura, N., and Iwabuchi, M. (2010) Genome-wide identification of a large repertoire of *Ralstonia solanacearum* type III effector proteins by a new functional screen. *Mol. Plant-Microbe Interact.* **23**, 251–262
59. Kim, J.-G., Park, B. K., Yoo, C.-H., Jeon, E., Oh, J., and Hwang, I. (2003) Characterization of the *Xanthomonas axonopodis* pv. *glycines* Hrp pathogenicity island. *J. Bacteriol.* **185**, 3155–3166
60. Büttner, D., Gürlebeck, D., Noël, L. D., and Bonas, U. (2004) HpaB from *Xanthomonas campestris* pv. *vesicatoria* acts as an exit control protein in type III-dependent protein secretion. *Mol. Microbiol.* **54**, 755–768
61. Kvitko, B. H., Ramos, A. R., Morello, J. E., Oh, H.-S., and Collmer, A. (2007) Identification of harpins in *Pseudomonas syringae* pv. *tomato* DC3000, which are functionally similar to HrpK1 in promoting translocation of type III secretion system effectors. *J. Bacteriol.* **189**, 8059–8072
62. Choi, M.-S., Kim, W., Lee, C., and Oh, C.-S. (2013) Harpins, multifunctional proteins secreted by gram-negative plant-pathogenic bacteria. *Mol. Plant-Microbe Interact.* **26**, 1115–1122
63. Monteiro, F., Solé, M., van Dijk, I., and Valls, M. (2012) A chromosomal insertion toolbox for promoter probing, mutant complementation, and pathogenicity studies in *Ralstonia solanacearum*. *Mol. Plant-Microbe Interact.* **25**, 557–568